coatings

MDPI

Article

Mathematical Modeling and Analysis of the Steady Electro-Osmotic Flow of Two Immiscible Fluids: A Biomedical Application

Haifa A. Alyousef [1], Humaira Yasmin [2,*], Rasool Shah [3], Nehad Ali Shah [4], Lamiaa S. El-Sherif [5] and Samir A. El-Tantawy [6,7]

1 Department of Physics, College of Science, Princess Nourah bint Abdulrahman University, P.O. Box 84428, Riyadh 11671, Saudi Arabia
2 Department of Basic Sciences, Preparatory Year Deanship, King Faisal University, Al-Ahsa 31982, Saudi Arabia
3 Department of Mathematics, Abdul Wali Khan University Mardan, Mardan 23200, Pakistan
4 Department of Mechanical Engineering, Sejong University, Seoul 05006, Republic of Korea
5 Department of Physics, College of Arts and Science in Wadi Al-Dawaser, Prince Sattam Bin Abdulaziz University, Wadi-Dawaser 11991, Saudi Arabia
6 Department of Physics, Faculty of Science, Port Said University, Port Said 42521, Egypt
7 Research Center for Physics (RCP), Department of Physics, Faculty of Science and Arts, Al-Mikhwah, Al-Baha University, Al-Baha 1988, Saudi Arabia
* Correspondence: hhassain@kfu.edu.sa

Abstract: The in vitro fabrication of big osteoarticular implants integrating biomaterials and cells is of tremendous interest because these tissues have a limited ability to regenerate. However, the growth of such cells in vitro is highly problematic, especially later in the culture, when the extracellular matrix has almost filled the initial porous network. Thus, the fluid flow required to properly perfuse the sample cannot be obtained by the hydraulic driving force alone. Fluid pumping is a central concern of a microfluidic system and electro-osmotic pumps (EOPs) are commonly employed for this purpose. Using electro-kinetic equations as a basis, this study analyzed the variations of a two-fluid electro-osmotic flow of viscoelastic fluid flow through a channel. The behavior of the fluid was studied through the Ellis equation. This is how the electro-osmotic pump functions, as demonstrated in the literature that it electrically drags a conducting fluid across a non-conducting fluid through interfacial dragging force along the channel. A steady-state analytical solution for the system in a conducting fluid channel was studied by undertaking an interface planner for fluids exhibiting Newtonian rheological properties. The pumping characteristics were studied in detail by using the Ellis model's parameters. The fluid rheology was studied, which showed the viability of this technique.

Keywords: mathematical modeling; electro-osmotic flow; two immiscible fluids; Ellis model

check for updates

Citation: Alyousef, H.A.; Yasmin, H.; Shah, R.; Shah, N.A.; El-Sherif, L.S.; El-Tantawy, S.A. Mathematical Modeling and Analysis of the Steady Electro-Osmotic Flow of Two Immiscible Fluids: A Biomedical Application. *Coatings* **2023**, *13*, 115. https://doi.org/10.3390/coatings13010115

Academic Editor: Jinyang Xu

Received: 7 November 2022
Revised: 1 January 2023
Accepted: 3 January 2023
Published: 8 January 2023

1. Introduction

Electro-osmotic flows have been subjected to recent investigation due to their application in electro-osmotic pumps, micro-reactors, micro-energy systems and micro-electronic cooling systems [1]. In these micro-channel networks, fluid pumps are used, in which the fluid is transported by an ion-dragging effect known as electro-osmosis. The review carried out by Wang et al. [2] on various studies regarding electro-kinetic pumps is related to a single-phase fluid, which is transported by a high electrical potential, with the help of a classical electro-osmotic pump. Therefore, the classical electro-osmotic flow pumping mechanism cannot be used for low electrical conductivity fluids. A new mechanism was suggested to overcome this limitation by Brask et al. [3]. They used a highly conducting electrolyte fluid to drag the low conductivity fluid. The non-Newtonian fluids with the highest electro-osmotic fluxes have also been the subject of recent investigations. In this regard, the power-law model was recently utilized [4,5]. They were successful in obtaining the exact relationships for the distributions of velocity, temperature, and concentration. The viscoelastic Phan-Thien and Tanner (PTT) and the finitely extendable nonlinear elastic-Peterlin (FENE-P) models have been used recently by Afonso et al. [6] to investigate the electro-osmotic flows in channel and pipe geometries. In addition, an earlier numerical study by Park and Lee [7], which was based on the PTT model with EOF in a square cavity, is also worth mentioning. These investigations were carried out by considering small EDL, in which a microfluidic device's walls are separated from one another by a distance that is greater than the EDL [6,7]. Due to the combined electric and pressure effects, the velocity profile exhibited an additional term (which also contributed to the total flow rate), which could be observed in non-Newtonian cases. In contrast, for Newtonian fluids, there was no such extra term and, thus, the superposition principle was applicable. Sousa et al. [8] further extended the study of viscoelastic models for pushing the zeta potential asymmetrically. Dhinakaran et al. [9] thought about a skimming layer that was low in polymer and located close to the walls. Dhinakaran et al. conducted an investigation into the pure EOF, with a non-zero second normal stress differential and a lack of a pressure difference. [10]. The fully developed electro-osmosis-driven flow of the SPTT or FENE-P models in a Newtonian solvent was also addressed by Afonso et al. [11]. Most recently, Martínez et al. [12] discussed the two-fluid electro-osmotic flow model via the simplify PTT model. The flow fluid rheology and pump ability were studied in detail under the influence of various relevant dimensionless parameters. An analysis of the two immiscible power–electro-osmotic law's flow by Deng et al. [13]. discussed fluids in a micro-channel [13]. Mustafa et al. [14] investigated heat transfer and Eyring–Powell fluid flow through a circular pipe. Foreseeing the effects of shear-thinning and yield stress, the Ellis fluid model is a generalized Newtonian fluid model. It is claimed that the power law and the Bingham model are subsets of this overarching paradigm. [15]. At extremely high shear loads, this model's results were identical to those of the power law model, while at moderate shear stresses, its behavior was similar to that of the Newtonian model. Therefore, the Ellis model is a helpful framework for evaluating the characteristics of different bio-fluids, such as blood, respiratory mucus, chime and cervical mucus, as it outperforms the Power law [16], the Newtonian law [17] and the Bingham Law models. The purpose of this article was to provide supplementary evidence to the findings of Afonso et al. [11], by including the Ellis model.

2. Flow Geometry

The governing flow equation is modeled using equations of mass and momentum. The body force term is incorporated using the well-known Poisson equation for electric potential. The analytical solution of the governing flow equation is presented in this paper, and graphical results are displayed and discussed for several values of the involved parameters.

The time-independent flow of two layers of immiscible viscoelastic fluid was under consideration in this study. A schematic of the flow configuration is introduced in Figure 1a. Such a flow situation can be encountered in some EOP pumps, in which there are two layers of conducting and non-conducting fluids. The electrically non-conducting liquid was in the upper half (Fluid A), while the electrically conducting liquid occupied the lower half (Fluid B) of the channel. This was because the electrically conducting liquid carries the electrically non-conducting liquid. This situation is demonstrated in Figure 1b. The movement of ions resulting in the development of electric double layers (EDLs) was, naturally, expected in the presence of an electrically conducting liquid and a dielectric wall. The process of the formation of EDLs is explained as follows: The lower charged channel wall attracts the opposite ions, forming a thin layer of electrically conducting liquid in the vicinity of the wall and pushing away the co-ions. This layer is called the stern layer. A more thickly diffuse layer of moving opposite ions succeeds the stern layer. The two layers formed in this way result in the EDLs. Next, when a DC and an external force are applied across the channel, then an external electric field is created, and, thus, the opposite ions of the EDLs accelerate near the bottom wall. As a result of the motion of these ions, the neutral liquid in the core is also dragged along the wall by the viscous effect. In the same manner, a second EDL is formed due to the dielectric interaction of the fluids at their interface in the charged fluid (near the interface). The external electric field is what causes the electrically conducting liquid to move, and the electrically non-conducting liquid is dragged by the conducting liquid as a result of the viscous effect at the interface. An external pressure gradient can also be added at the ends of the channel. The direction of the action of pressure can be either along the direction of the external body force or vice versa. We placed the origin of the frame of reference at (x, y), when the two fluids meet at their interface. The thickness of Fluid A and Fluid B is denoted by H_1 and H_2, respectively. It was further assumed that width, W, was supposed to be $W >> H_1 + H_2 = H$. Furthermore, the holdup of the fluid in the lower half was given by the following:

$$R_B = \frac{H_1}{(H_1 + H_2)} = \frac{H_1}{H}, \tag{1}$$

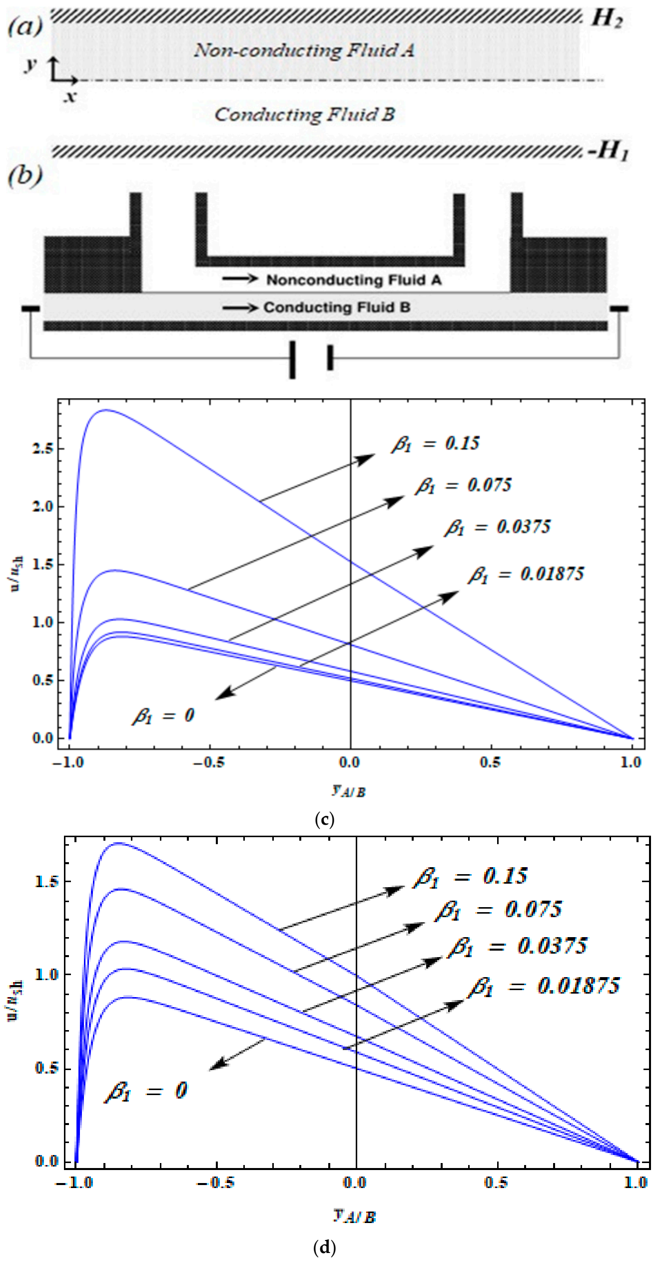

Figure 1. (**a**) Schematic diagram of flow geometry in a channel. (**b**) The diagram of EOF pump. (**c**) $\beta = 1; \Gamma = 0; R = 20; R_\zeta = 0; R_A = \frac{1}{2}$; (**d**) $\beta = 1; \Gamma = 0; R = 20; R_\zeta = 0; R_A = \frac{1}{2}$.

This is, in fact, the ratio of the cross-sectional area of Fluid B to the total cross-sectional area of the channel. In the same manner, the holdup of the fluid in the upper half was given by the following:

$$R_A = 1 - R_B = \frac{H_2}{H_1 + H_2} = \frac{H_2}{H}, \tag{2}$$

The zeta potential of the EDL that formed near the bottom wall is denoted by ζ_1, while ζ_i stands for the zeta potential of the EDL that formed at the interface. The equation [16–18],

$$\frac{\partial \rho}{\partial t} + \nabla.\rho u \tag{3}$$

is known as the continuity equation. In Equation (3), ρ is the density, u is the fluid velocity and t is the time. When flow is incompressible, the above equation becomes the following:

$$\nabla.u = 0 \tag{4}$$

The equation of motion can be expressed as follows, in which b is the body force per unit volume and σ is the Cauchy stress tensor [18]:

$$\rho \frac{du}{dt} = \nabla.\sigma + \rho b. \tag{5}$$

2.1. Potential Field for Fluid B

The flow under consideration was steady and fully developed. The potential difference inside the charged Fluid B was obtained using the Poisson equation. A potential field is created by the charge, so, in this study, we could relate the potential field and charge density by a divergence relationship. This relationship is a combination of Maxwell's equation and vector calculus operation, known as divergence [17]. The divergence of the electric potential at some point is equal to the charge density divided by the dielectric constant of the material, i.e., as follows:

$$\nabla.E = \frac{\rho_e}{\in} \tag{6}$$

The expression of the electric potential in terms of voltage can be expressed in vector form, as follows:

$$E = -\frac{\partial \psi}{\partial x} i - \frac{\partial \psi}{\partial y} j - \frac{\partial \psi}{\partial z} k \tag{7}$$

$$E = -\nabla \psi \tag{8}$$

By substituting Equation (8) into Equation (6), the following is obtained:

$$\nabla^2 \psi = -\frac{\rho_e}{\in}. \tag{9}$$

Equation (9) is known as the Poisson equation for electric potential. The expression of ρ_e for the electrolyte solution in equilibrium in the neighborhood of a charged wall is as follows:

$$\rho_e = -2n_\circ ez \sinh\left(\frac{ez}{k_B T}\psi\right) \tag{10}$$

where $n_\circ, e, z, k_B$ and T are the density of the ions, electric charge, active ions, Boltzmann constant and temperature, respectively [11].

To obtain the velocity field inside *Fluid B*, the net charge density, ρ_e, had to be calculated beforehand. Using a combination of Equations (9) and (10), under the assumption that the flow was fully developed, we obtained the following:

$$\frac{d^2\psi}{dy^2} = \frac{2n_\circ ez}{\in} \sinh\left(\frac{ez}{k_B T}\psi\right). \tag{11}$$

Equation (11) is a well-known Poisson–Boltzmann equation. The application of the Debye–Huckel linearization principle gave us the following:

$$\frac{d^2\psi}{dy^2} = k^2\psi, \tag{12}$$

where $k^2 = \frac{-2n_\circ e^2 z^2}{\in k_B T}$ is the Debye–Huckel coefficient. The parameter, k, is related to the Debye thickness, λ_D, as $\lambda_D = \frac{1}{k}$. The above approximation holds for a small Debye thickness, i.e., for $10 < kH < 10^3$. As an implication, the induced potential and its energy remain small. Physically, the Deby–Huckel principle means that electric potential energy is small in comparison to the thermal energy of ions. Given the appropriate boundary conditions, we can solve Equation (12).

$$\psi_{y=-H_i} = \zeta_1, \psi_{y=0} = \zeta_i.$$

The solution of Equation (12) is as follows:

$$\psi(y) = \zeta_1\left(\psi_1 e^{ky} - \psi_2 e^{-ky}\right), \tag{13}$$

where

$$\psi_1 = \frac{R_\zeta e^{kH_1} - 1}{2\sinh(kH_1)}, \psi_2 = \frac{R_\zeta e^{-kH_1} - 1}{2\sinh(kH_1)}, R_\zeta = \frac{\zeta_i}{\zeta_1}.$$

The case $R_\zeta = 1$, corresponding to the symmetric potential profile was examined by Afonso et al. [5]. In another attempt, Afonso et al. [7] also discussed the case for vanishing zeta potential.

In view of Equation (11), the charge density, ρ_e, becomes the following:

$$\rho_e = - \in k^2\zeta_1\left(\psi_1 e^{ky} - \psi_2 e^{-ky}\right) = - \in k^2\zeta_1\Omega_1^-(y), \tag{14}$$

where

$$\Omega^\pm(y) = \left(\psi_1 e^{ky}\right)^p \pm \left(\psi_2 e^{-ky}\right)^p,$$

is an exponential function that is dependent on both the zeta potential and the Debye layer's width. Both the potential and the related charge density were zero for the non-conducting Fluid A.

2.2. Governing Equations and the Rheological Model

The equations governing the flow problem under investigation are Equations (4) and (5). In the present scenario, the body force term was $\rho_e E$, therefore, the momentum equation was the following:

$$\rho\frac{du}{dt} = -\nabla P + \nabla.\sigma + \rho_e E. \tag{15}$$

where $E = -\nabla\phi$ the applied electrostatic and ρ_e is the net electrostatic charge density. The term $\rho_e E$ in Equation (2) was zero for the electrically non-conducting liquid. The constitutive model that was used in this study to represent the visco-elastic characteristics of the fluid was the Ellis model, for which the τ satisfies [18] the behavior of fluid in both regions and is characterized by the constitutive equation of the Ellis model. For Ellis's model, the constitutive equation is as follows:

$$\tau = 2\eta(\tau)D, \tag{16}$$

where,

$$\eta(\tau) = \frac{n_\circ}{1 + \left(\frac{\tau}{\tau_\circ^2}\right)^{\alpha-1}} \tag{17}$$

and where τ is the magnitude of the extra stress tensor given by

$$\tau = |\tau| = \sqrt{\frac{1}{2}}(\tau : \tau). \tag{18}$$

$\tau_\circ$ and α are materials constant, $D = \frac{(\nabla u^T + \nabla u)}{2}$ is the rate of deformation tensor and $\eta_\circ$ is the zero-shear rate viscosity. The continuity of Equation (3) for the present flow problem — for which $u = [u(y), 0, 0]$ — was satisfied identically, while the momentum in Equation (5) for conducting Fluid B became the following:

$$\tau_{xy,B} = P_{xy} + \in k\zeta E_x \Omega_1^+(y) + \tau_B. \tag{19}$$

In the above equation the component of the extra stress tensor, τ_{xy}, satisfies the following equation:

$$\tau_{xy} = \frac{\eta \frac{du_B}{dy}}{1 + \left(\frac{\tau_{xy}}{\tau_\circ^2}\right)^{\alpha - 1}}. \tag{20}$$

By substituting Equation (19) into Equation (20) and rearranging, we obtained the following:

$$\eta \frac{du_B}{dy} = \left(P_{xy} + \in k\zeta E_x \Omega_1^+(y) + \tau_B\right) + \left(\frac{1}{\tau_\circ^2}\right)^{\alpha - 1} \left(P_{xy} + \in k\zeta E_x \Omega_1^+(y) + \tau_B\right)^{\alpha}. \tag{21}$$

The integration of the above equation was performed for arbitrary, α. Therefore, we shall give the results for some specific values of α.

For $\alpha = 1$, Equation (21) can be integrated using the boundary condition $u_B = 0$ at $y = -H_1$ to give the result in the dimensionless form

$$\bar{k} = kH_1, \bar{y} = \frac{y}{H_1}, \bar{\tau}_B = \frac{\tau_B R_B H}{\eta u_{sh}}, De_k = \lambda k u_{sh}, \Gamma = \frac{-(R_B H)^2 P_x}{\in \zeta_1 E_x}.$$

For brevity, we are defining $\varepsilon = \varepsilon_B, \eta = \eta_B$, where

$$\begin{aligned} \Omega_{a,b}(y) &= (ky)^{b-1}\Omega_a^{\pm}(y) - (-1)^{(b+1)}(kH_1)^{(b-1)}\Omega_a^{\pm}(-H_1). \\ \tfrac{u_B}{u_{sh}} &= \Gamma_B\left(\bar{y}^2 - 1\right) + 2\bar{\tau}_B(\bar{y} + 1) - 2\Omega_{1,1}^-(y). \end{aligned} \tag{22}$$

Similarly, for $\alpha = 2, 3$, one can easily find the following:

$$\begin{aligned} \tfrac{u_B}{u_{sh}} = 2\bar{k}^2\psi_1\psi_2\beta_1(\bar{y}+1) + \tau_B(\bar{y}+1) + \bar{\tau}_B^2\beta_1(\bar{y}+1) - \Omega_{1,1}^-(y) \\ -2\tau_B\beta_1\Omega_{1,1}^-(y) - \tfrac{2\beta_1\Gamma}{\bar{k}}\Omega_{2,1}^-(y) + \tfrac{\Gamma}{2}\left(\bar{y}^2 - 1\right) + \beta_1\Gamma\tau_B\left(\bar{y}^2 - 1\right) \\ + \tfrac{\beta_1\Gamma^2}{3}\left(\bar{y}^3 + 1\right) + \tfrac{2\beta_1\Gamma}{\bar{k}}\Omega_{1,1}^+(y) + \tfrac{1}{2}\bar{k}\beta_1\Omega_{2,1}^-(y) \end{aligned} \tag{23}$$

$$\begin{aligned} \frac{u_B}{u_{sh}} = \frac{\Gamma_B}{2}\left(\bar{y}^2 - 1\right) + \bar{\tau}_B(\bar{y}+1) + \frac{3\beta_1^2\Gamma_B\bar{\tau}_B^2}{2}\left(\bar{y}^2 - 1\right) + \beta_1^2\bar{\tau}_B^3(\bar{y}+1) - \Omega_{1,1}^-(y) \\ + \frac{6\beta_1^2\Gamma_B^2}{\bar{k}}\left(\Omega_{2,1}^+(y) - \Omega_{1,1}^-(y)\right) - 3\beta_1^2\Gamma_B^2\Omega_{2,2}^-(y) - 3\beta_1^2\bar{\tau}_B^2\Omega_{1,1}^-(y) \\ + 3\beta_1^2\Gamma_B\bar{k}\psi_1\psi_2\left(\bar{y}^2 - 1\right) + 6\beta_1^2\bar{k}^2\bar{\tau}_B\psi_1\psi_2(\bar{y}+1) \\ + \frac{3\beta_1^2\Gamma_B}{2}\left(\Omega_{1,3}^-(y) - \frac{\Omega_{1,3}^-(y)}{2}\right) + \frac{3\beta_1^2\bar{k}\bar{\tau}_B}{2}\Omega_{2,1}^-(y) \\ - \frac{\beta_1^2\bar{k}^2}{3}\Omega_{3,1}^-(y) - 3\beta_1^2\bar{k}^2\psi_1\psi_2\Omega_{1,1}^-(y) \end{aligned} \tag{24}$$

The volumetric flow rate of Fluid B for $\alpha = 1,2,3,$ was calculated by integrating Equations (22)–(24). This gave us the following:

$$\overline{Q}_B = \int_{-1}^{0} \frac{u_B}{u_{sh}} d\overline{y} = \overline{\tau}_B - \frac{2}{3}\Gamma_B + 2\Omega_1^-(-1) - \frac{2}{\overline{k}}\Omega_{1,1}^+(0), \alpha = 1 \tag{25}$$

$$\begin{aligned}\overline{Q}_B = \int_{-1}^{0} \frac{u_B}{u_{sh}} d\overline{y} =& \overline{k}^2\beta_1\psi_1\psi_2 - \frac{\Gamma_B}{3} + \frac{\beta_1\Gamma_B^2}{4} + \frac{\tau_B}{2} - \frac{2\beta_1\Gamma_B\tau_B}{3} \\ &+ \frac{\beta_1\tau_B^2}{2}\Omega_1^-(-1) + \frac{\Omega_{1,1}^+(0)}{\overline{k}} - 2\beta_1\Gamma_B\Omega_1^-(-1) \\ &+ \frac{4\beta_1\Gamma_B}{\overline{k}^2}\left(\Omega_1^-(0) + \Omega_1^-(-1)\right) - \frac{4\beta_1\Gamma_B}{\overline{k}}\Omega_1^+(-1) \\ &+ 2\beta_1\tau_B\Omega_1^-(-1) - \frac{2\beta_1\tau_B}{\overline{k}}\left(\Omega_1^+(0) + \Omega_1^+(-1)\right) \\ &+ \frac{\beta_1}{4}\left(\Omega_2^+(0) - \Omega_2^+(-1)\right) - \frac{\overline{k}\beta_1}{2}\Omega_2^+(-1), \alpha = 2\end{aligned} \tag{26}$$

$$\begin{aligned}\overline{Q}_B = \int_{-1}^{0} \frac{u_B}{u_{sh}} d\overline{y} =& \frac{\tau_B}{2} + 3\overline{k}^2\beta_1^2\tau_B\psi_1\psi_2 + \frac{\beta_1^2\tau_B^3}{2} - \frac{\Gamma_B}{3} - 2\overline{k}^2\beta_1^2\Gamma_B\psi_1\psi_2 \\ &- \beta_1^2\tau_B^2\Gamma_B + \frac{3\beta_1^2\tau_B\Gamma_B^2}{4} - \frac{\beta_1^2\Gamma_B^3}{5} - \frac{\Omega_{1,1}^+(0)}{\overline{k}} \\ &- 3\overline{k}\beta_1^2\psi_1\psi_2\Omega_{1,1}^+(0) + 3\overline{k}^2\beta_1^2\psi_1\psi_2\Omega_1^-(-1) \\ &+ 3\beta_1^2\tau_B\Omega_1^-(-1) + \frac{\beta_1^2\tau_B^2}{\overline{k}}\Omega_{1,1}^+(0) - 6\beta_1^2\tau_B\Gamma_B\Omega_1^-(-1) \\ &+ \frac{12\beta_1^2\tau_B\Gamma_B}{\overline{k}^2} \times \left(\Omega_{1,1}^-(0) - \Omega_1^+(-1)\right) + 3\beta_1^2\Gamma_B^2\Omega_1^-(-1) \\ &- \frac{18\beta_1^2\Gamma_B^2}{\overline{k}^3}\Omega_{1,1}^+(0) + \frac{18\beta_1^2\Gamma_B^2}{\overline{k}^2}\Omega_1^-(-1) \\ &+ \frac{9\beta_1^2\Gamma_B^2}{\overline{k}}\Omega_1^+(-1) + \frac{3\beta_1^2\tau_B}{4} \times \left(\Omega_2^+(0) - \Omega_2^+(-1)\right) \\ &+ \frac{3\beta_1^2\Gamma_B}{2}\Omega_2^-(-1) - \frac{3\beta_1^2\Gamma_B}{4\overline{k}}\Omega_{2,1}^-(0) + \frac{3\overline{k}\beta_1^2\Gamma_B}{2}\Omega_2^+(-1) \\ &+ \frac{\overline{k}^2}{9}\left(\Omega_3^+(-1) - \Omega_3^+(0)\right) - \frac{3\overline{k}\beta_1^2\tau_B}{2}\Omega_2^-(-1) \\ &+ \frac{\overline{k}^2\beta_1}{3}\Omega_3^-(-1), \alpha = 3\end{aligned} \tag{27}$$

The momentum in Equation (5) for non-conducting fluid A was as follows:

$$\tau_{xy,A} = P_{xy} + \tau_A \tag{28}$$

By substituting Equation (28) into Equation (20) and rearranging, we arrived at the following equation:

$$\eta\frac{du_A}{dy} = \left(P_{xy} + \tau_A\right) + \left(\frac{1}{\tau_\circ^2}\right)^{\alpha-1}\left(P_{xy} + \tau_A\right)^\alpha \tag{29}$$

Again, the integration of the above equation was performed for arbitrary, α. Therefore, we shall give the results for some specific values of α. For $\alpha = 1$, Equation (29) was integrated using the boundary condition $u_A = 0$ at $y = H_2$, to give the following:

$$\frac{u_A}{u_{sh}} = 2\overline{\tau}_A(\overline{y}-1) + \frac{\Gamma_A}{\beta}\left(\overline{y}^2 - 1\right). \tag{30}$$

Similarly, the corresponding profiles for $\alpha = 2$ and 3 were as follows:

$$\frac{u_A}{u_{sh}} = \overline{\tau}_A(\overline{y}-1) + \frac{\Gamma_A}{2\beta}\left(\overline{y}^2 - 1\right) + \beta_1\overline{\tau}_A^2(\overline{y}-1) + \frac{\beta_1\overline{\tau}_A\Gamma_A}{\beta}\left(\overline{y}^2 - 1\right) + \frac{\beta_1^2\Gamma_A^2}{3\beta^2}\left(\overline{y}^3 - 1\right) \tag{31}$$

$$\begin{aligned}\tfrac{u_A}{u_{sh}} = \overline{\tau}_A(\overline{y}-1) + \tfrac{\Gamma_A}{2\beta}(\overline{y}^2 - 1) + \tfrac{\beta_1^2\Gamma_A^3}{4\beta^3} + \tfrac{\beta_1^2\Gamma_A^2\overline{\tau}_A}{\beta^3}(\overline{y}^3 - 1) + \tfrac{3\beta_1^2\Gamma_A\overline{\tau}_A^2}{2\beta^3}(\overline{y}-1) \\ +\beta_1^2\overline{\tau}_A^2(\overline{y}-1).\end{aligned} \tag{32}$$

The volumetric flow rate of Fluid A for $\alpha = 1, 2, 3$ was an expression of the following:

$$\overline{Q}_A = \int_0^1 \frac{u_A}{u_{sh}} d\overline{y} = -\overline{\tau}_A - \frac{2\Gamma_A}{3\beta}, \tag{33}$$

$$\overline{Q}_A = \int_0^1 \frac{u_A}{u_{sh}} d\overline{y} = -\frac{\Gamma_A}{3\beta} - \frac{\beta_1\Gamma_A^2}{4\beta^2} - \frac{\overline{\tau}_A}{2} - \frac{2\beta_1\Gamma_A\overline{\tau}_A}{3\beta} - \frac{\beta_1\overline{\tau}_A^2}{2}, \tag{34}$$

$$\overline{Q}_A = \int_0^1 \frac{u_A}{u_{sh}} d\overline{y} = -\frac{\overline{\tau}_A}{2} - \frac{\beta_1\overline{\tau}_A^2}{2} - \frac{\Gamma_A}{3\beta} - \frac{\beta_1^2\overline{\tau}_A^2\Gamma_A}{\beta^3} - \frac{3\beta_1\overline{\tau}_A^2\Gamma_A^2}{4\beta^3} + \frac{\beta_1^2\Gamma_A^3}{4\beta^3}. \tag{35}$$

It should be noted that the expressions of Equations (22)–(24) and Equations (30)–(32) still involve unknown constants. To determine these constants, we used interfacial conditions at $y = 0$, $\overline{\tau}_{xy,A} = \overline{\tau}_{xy,B}$ and $\overline{u}_A = \overline{u}_B$. The application of these conditions yielded algebraic equations in $\overline{\tau}_B$, which were solved analytically. Once $\overline{\tau}_B$ was known, $\overline{\tau}_A$ was computed through the following equation:

$$\overline{\tau}_A = \frac{R_A}{R_B}\frac{1}{\beta}\overline{\tau}_B - \frac{\overline{k}}{\beta}\Omega_1^+(0). \tag{36}$$

3. Results and Discussion

In this section, we analyze a special case in great depth to learn about the system's fluid dynamics. The generic solution applies to the classes of two-fluid systems consisting of Newtonian and non-Newtonian fluids; viscoelastic and non-Newtonian fluids; Newtonian and viscoelastic fluids; and viscoelastic and viscoelastic fluids. We will only discuss Case (c). In Case (c), the viscoelastic electrically conducting liquid dragged the electrically non-conducting Newtonian liquid behind it. The Deborah number, zero, describes the non-conducting fluid. The present finding is compatible with the analytical solution reported in the literature for the motion of Newtonian fluids. The dimensionless velocity for $\alpha = 3, 2$ is shown in Figure 1c,d. Here, we can see that if the conducting fluid's flexibility is increased, then the velocities multiply more as a result of activities that shear down the thickness of the EDL layer, which increases the bulk transport velocity value at the channel's core. This boosts the shear rates near the bottom wall, which increased as a result of the drag force exerted by the non-conducting fluid, which was brought about by hydrodynamic viscous forces at the interface. Figure 2a,b show the impact of Γ. When $\Gamma < 0$, then the flow rate increased and, thus, the velocity increased. To further boost the flow rate, the pressure force can be used to act directly on the two fluids. The dramatic improvement of this investigation is the evidence of the shear-thinning effect, which can be seen in the flow rate. The impact of the viscosity ratio on the dimensionless velocity profile is shown in Figure 3. Accordingly, we can see that the dimensionless velocity increased as the viscosity ratio decreased. Therefore, an increase in the dimensionless velocity can be predicted if the conducting fluid has a viscosity that is significantly higher than the electrically non-conducting liquid, as shown in this figure. However, a lower Helmholtz–Smoluchowski electro-osmotic velocity is implied by a larger viscosity, and, as a result, it is possible that the dimensional flow rate will go down. As we can observe in Figure 4's profiles, a non-zero interfacial zeta potential caused a significant difference in the surface charge, a favorable additional Columbic forcing term occurred, and, when $R_\zeta > 0$, a significant rise in the dimensionless velocity profile occurred. For small values of R_ζ, the pumping action and the associated dimensionless velocity were dampened by a detrimental, localized electrostatic force. The accumulation of electrically non-conducting liquid was another factor that had a considerable impact. As can be seen in Figure 5, the normalized velocities of both fluids increased when the electrically non-conducting liquid had a greater height than the conducting fluid $(R_A > R_B)$. The Helmholtz–Smoluchowski velocity does not dependent on Fluid B's holdup, and the regions with greater velocities tended to coincide with the fluid interface plane, as $R_A \to 1$. This analysis further implies that the best configuration for an EOF pump is a fluid flow with three layers in which the conducting fluid contacts only one of the other layers, where the motion of the smallest layers of conducting fluid can serve as a lubricant at the ends of the walls, and the non-conducting fluid is pulled, as a solid body. Figure 6 displays the variation of the volumetric flow rate and the velocity profile for the different values of the Ellis fluid parameters: α and β_1. It was observed that the effect of α was to decrease the velocity profile in both the conducting and non-conducting regions. Due to this decrease, the volumetric flow rate also followed a decreasing trend, with an increase in α. However, this decreasing trend prevailed up to a certain critical value of β_1 and, thereafter, the flow rate increased with an increasing in α. The viscosity ratio, $\beta = \left(\frac{\eta_A}{\eta_B}\right)$, affected the volumetric flow rate, as shown in Figure 7. Viscosity ratios decrease when the dimensionless volumetric flow rate increases, if the conducting fluid has a substantially higher viscosity than the non-conducting fluid. A decrease in the Helmholtz–Smoluchowski electro-osmotic velocity, however, can be predicted by increased viscosity and could result in a decrease in the dimensional flow rate. The dimensionless flow rate is clearly affected by the pressure gradient to the electro-osmotic driving force ratio, Figure 8, specifically, for flows where the pressure gradient is decreasing or where it is increasing. Since *Fluid B* was also being propelled by electro-osmosis at the same fluid height, its flow rate was obviously greater than that of *Fluid A.* As seen in Figure 9, in situations where the height of the conducting fluid was greater than that of the non-conducting fluid, keeping the holdup of the conducting fluid (*Fluid B*) to be a minimum, which it is necessary in order to increase the volumetric flow rates in *Fluid A*. As shown in the profiles of Figure 10, the interfacial zeta potential had a significant impact on the volumetric flow rate, which significantly increased when $\left(\frac{\zeta_i}{\zeta_1} > 0\right)$. The pumping action and the accompanying dimensionless flow rate were decreased due to the unfavorable, localized electrostatic force.

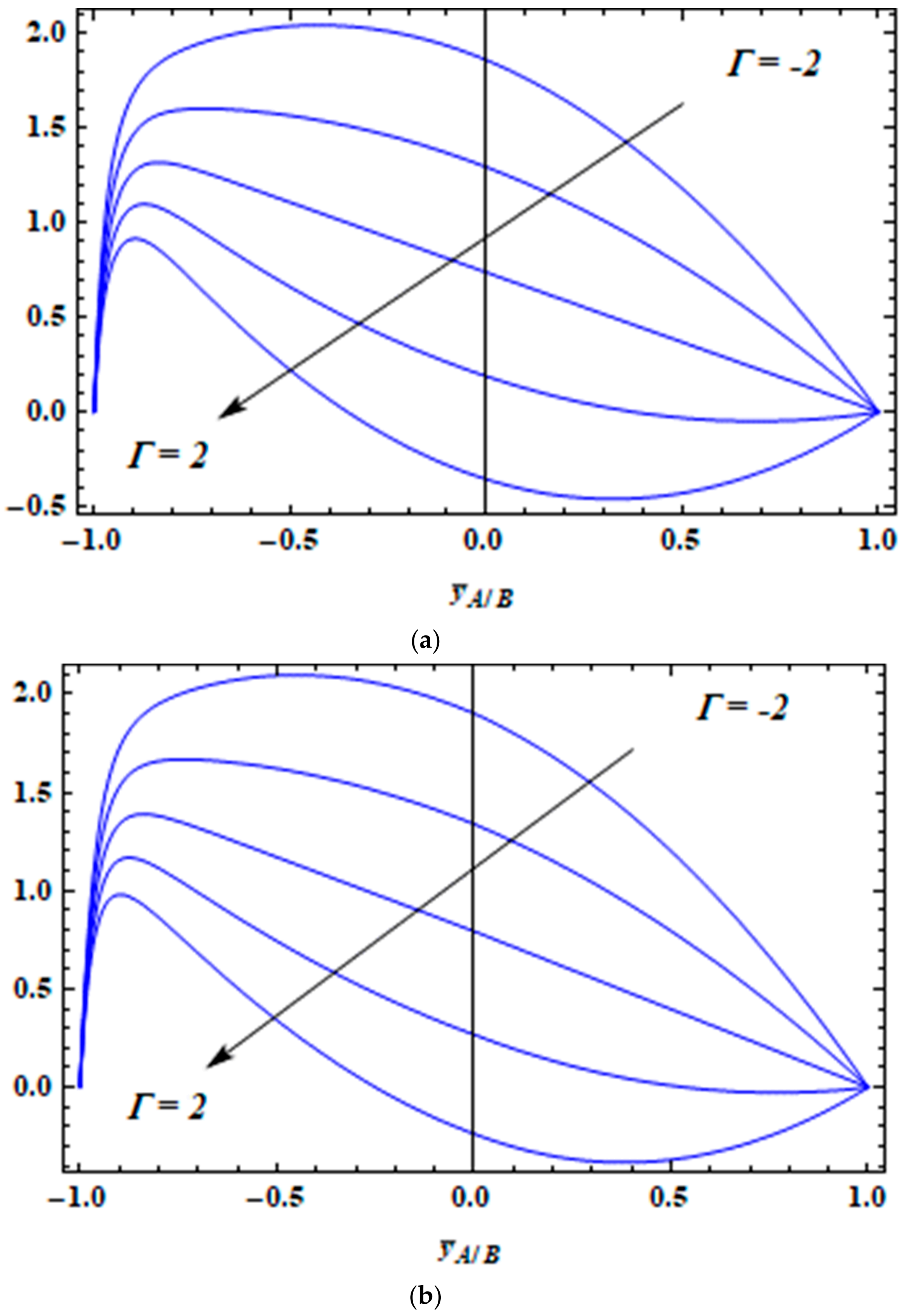

Figure 2. (**a**) $\beta = 1; R = 20; R_\zeta = 0; R_A = \frac{1}{2}$; (**b**) $\beta = 1; R = 20; R_\zeta = 0; R_A = \frac{1}{2}$.

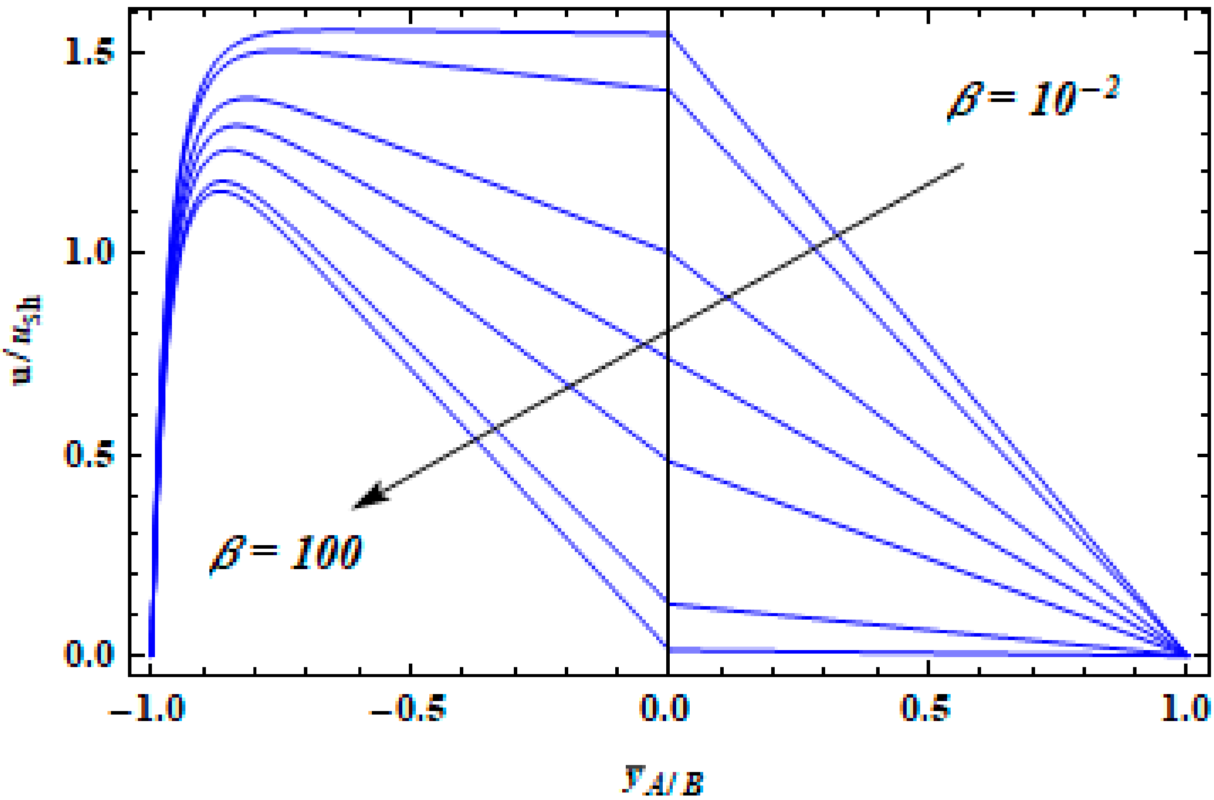

(**a**)

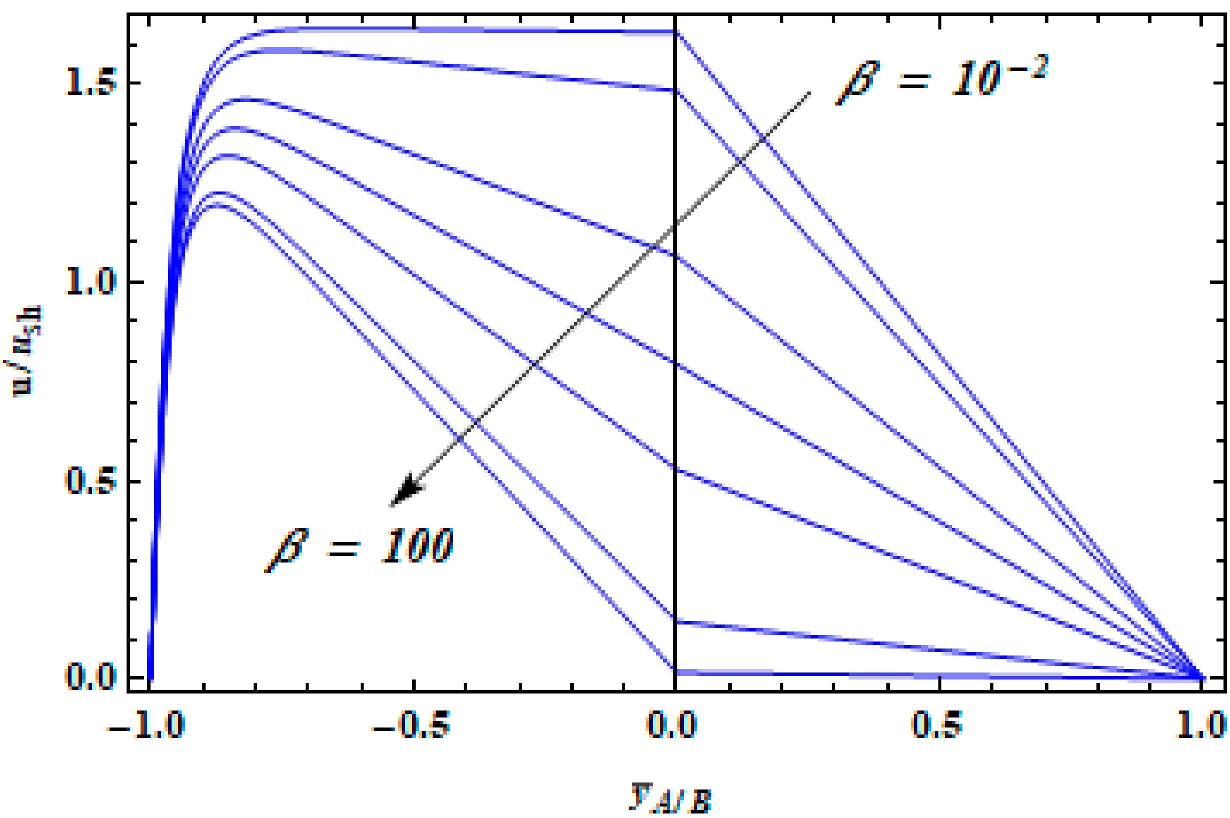

(**b**)

Figure 3. (**a**) $\beta = 1; \Gamma = 0; R = 20; R_\zeta = 0; R_A = \frac{1}{2}$; (**b**) $\beta = 1; \Gamma = 0; R = 20; R_\zeta = 0; R_A = \frac{1}{2}$.

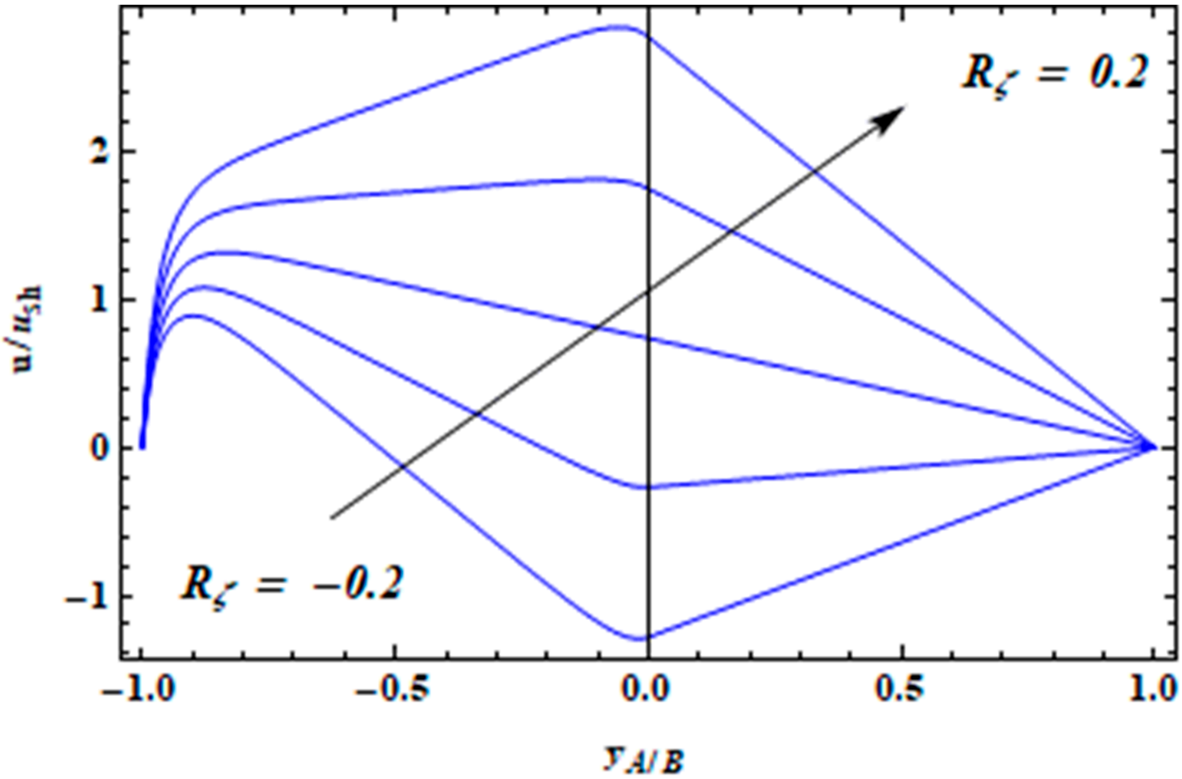

(**a**)

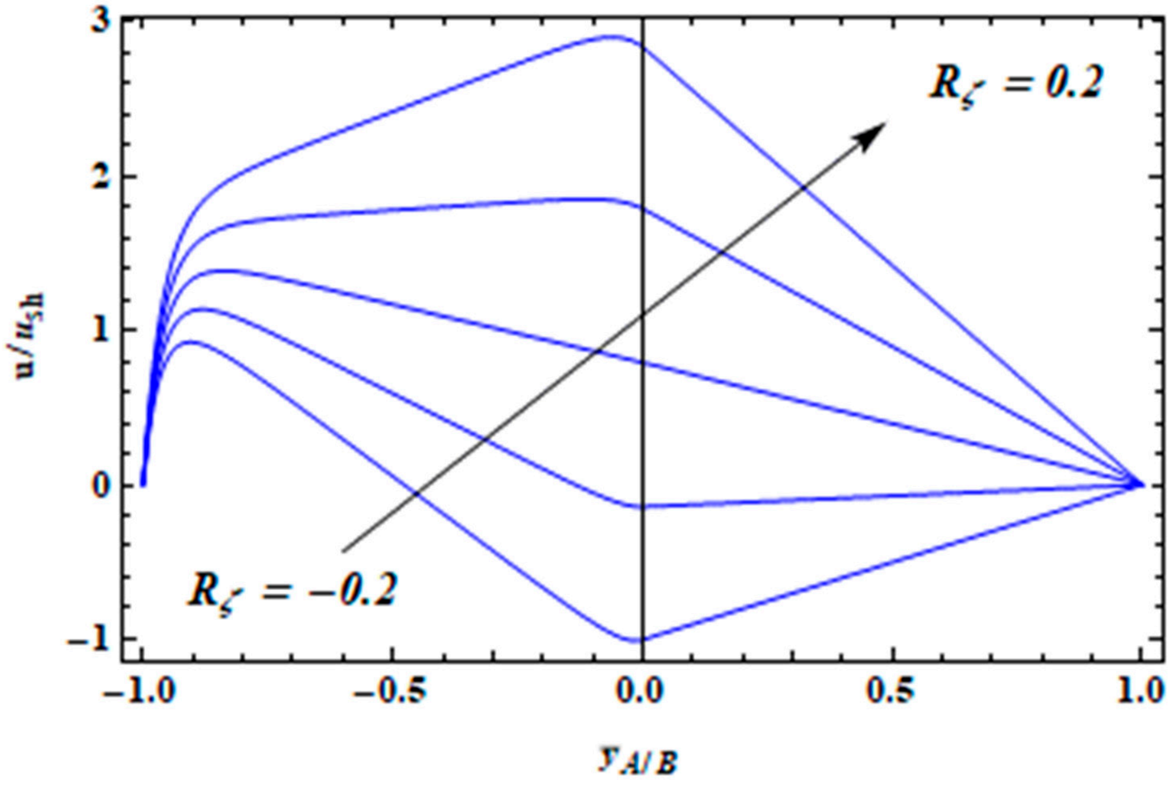

(**b**)

Figure 4. (**a**) $\beta = 1; \Gamma = 0; R = 20; R_A = \frac{1}{2}$; (**b**) $\beta = 1; \Gamma = 0; R = 20; R_A = \frac{1}{2}$.

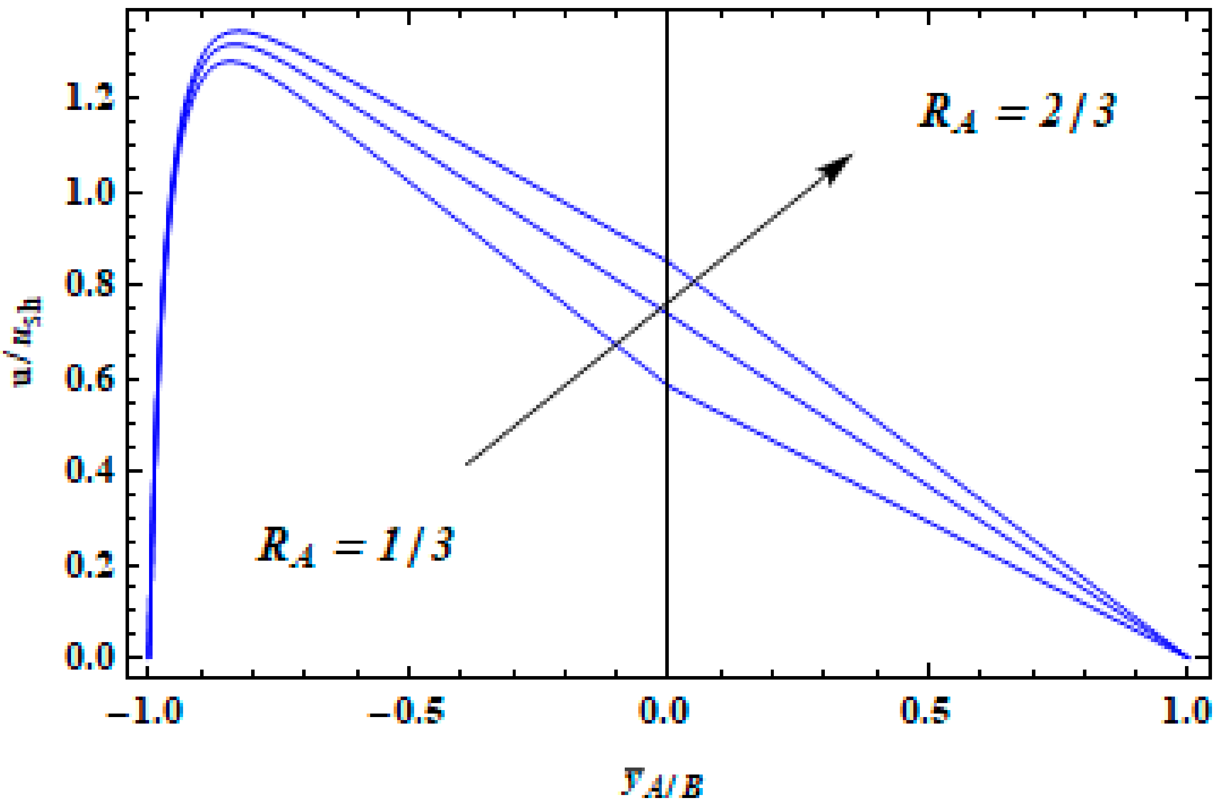

(**a**)

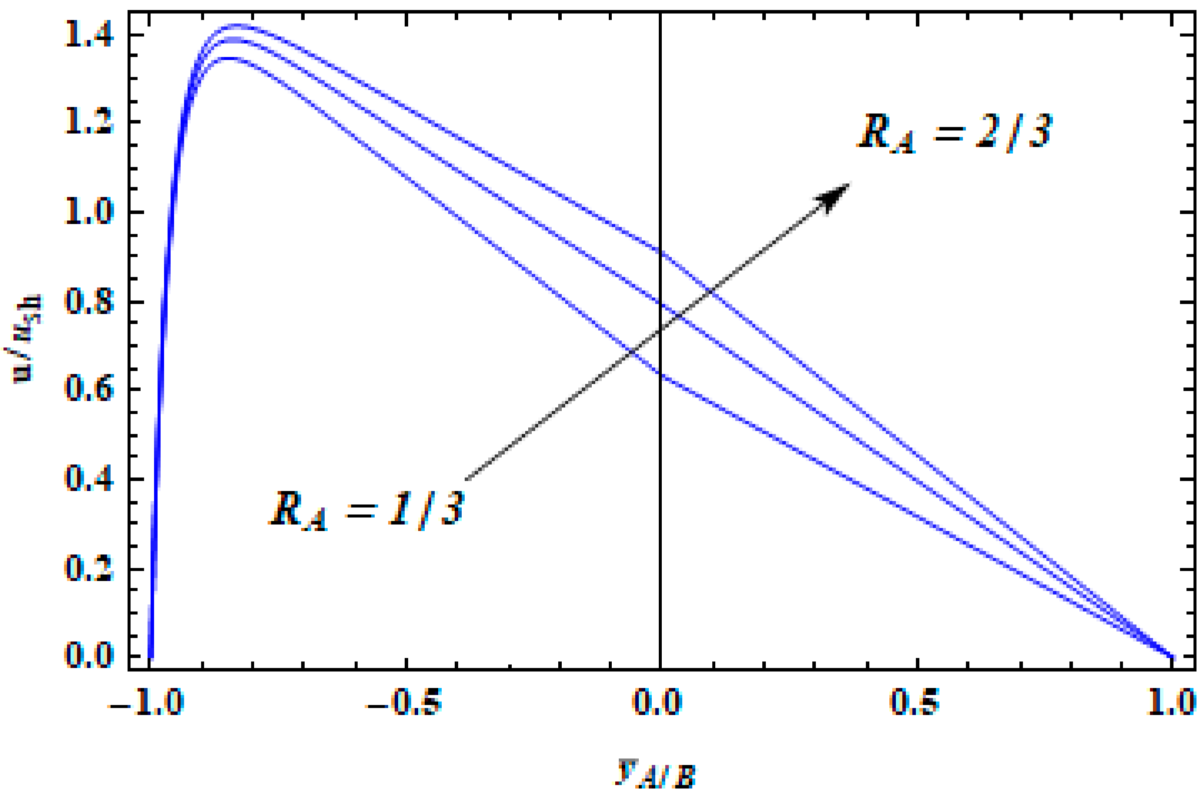

(**b**)

Figure 5. (**a**) $\beta = 1; \Gamma = 0; R_B = 0.2; k = 20; R_\zeta = 0$; (**b**) $\beta = 1; \Gamma = 0; R_B = 0.2; k = 20; R_\zeta = 0$.

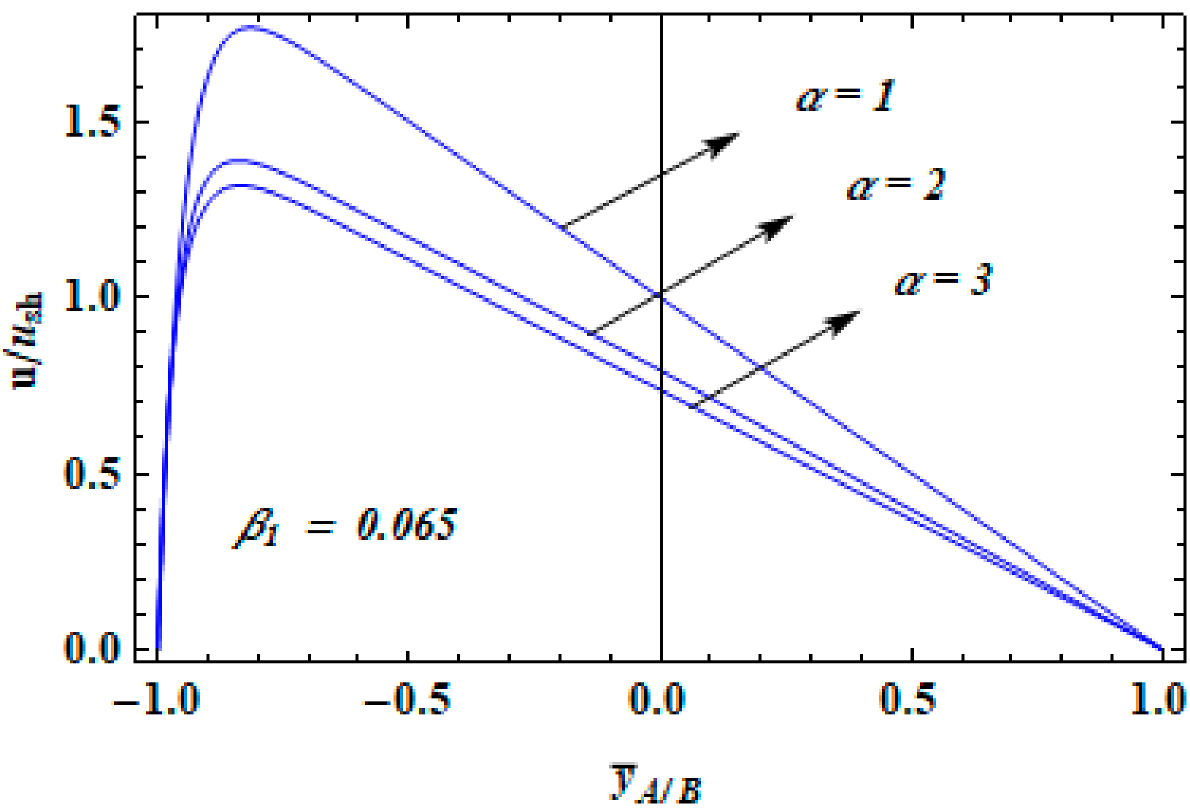

(**a**)

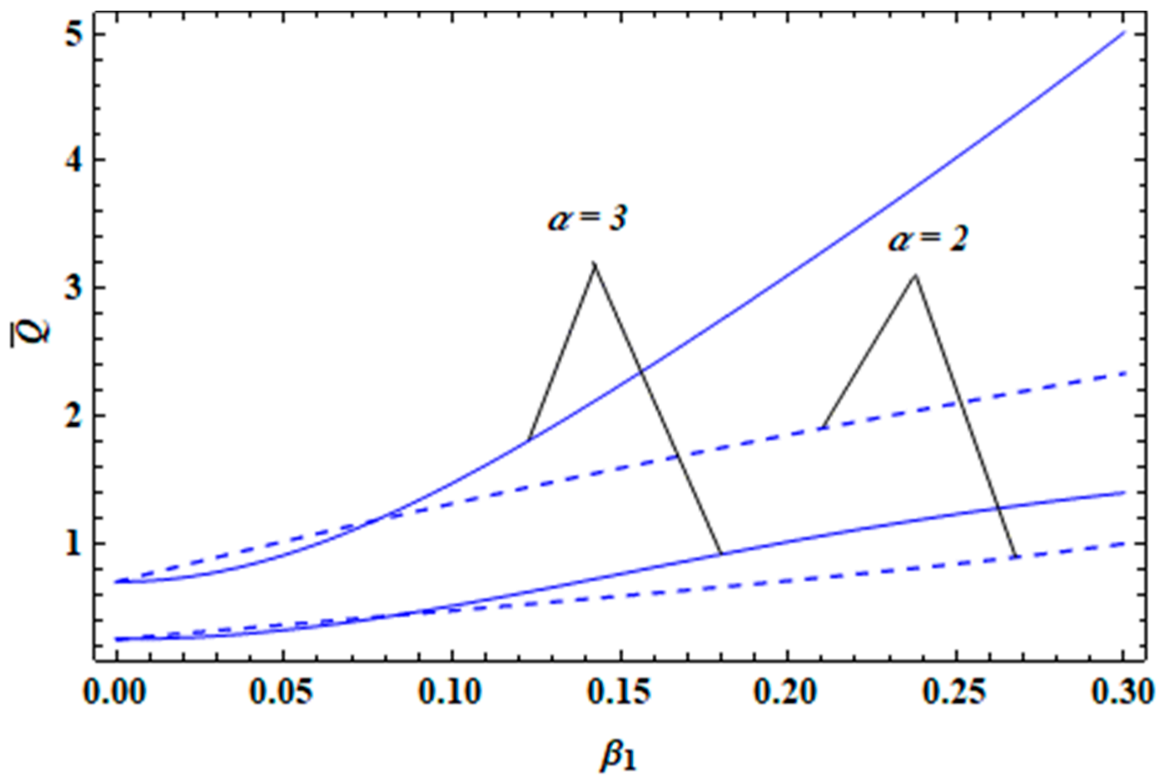

(**b**)

Figure 6. (**a**) $\beta = 1; \Gamma = 0; R_A = 0.2; k = 20; R_\zeta = 0$; (**b**) $\beta = 1; \Gamma = 0; R_A = 0.2; k = 20; R_\zeta = 0$.

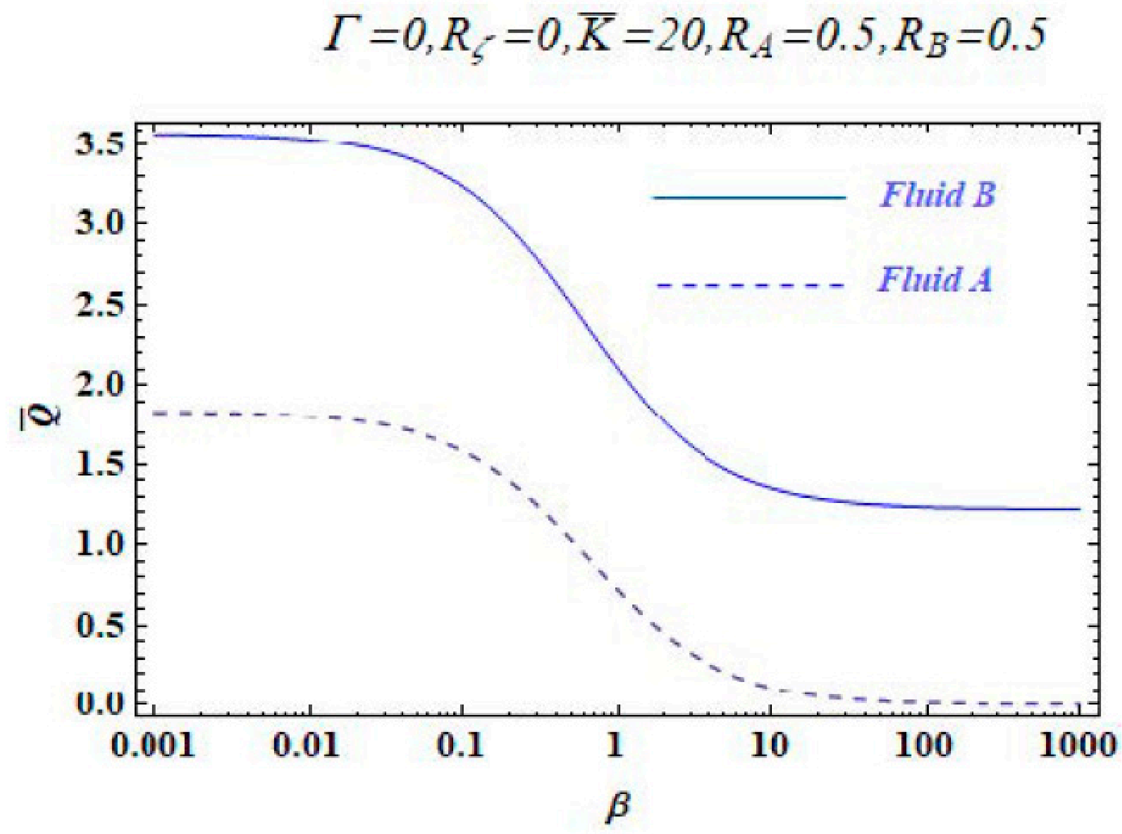

Figure 7. β *vs* $\overline{Q}$ for Fluid *A* and Fluid *B*.

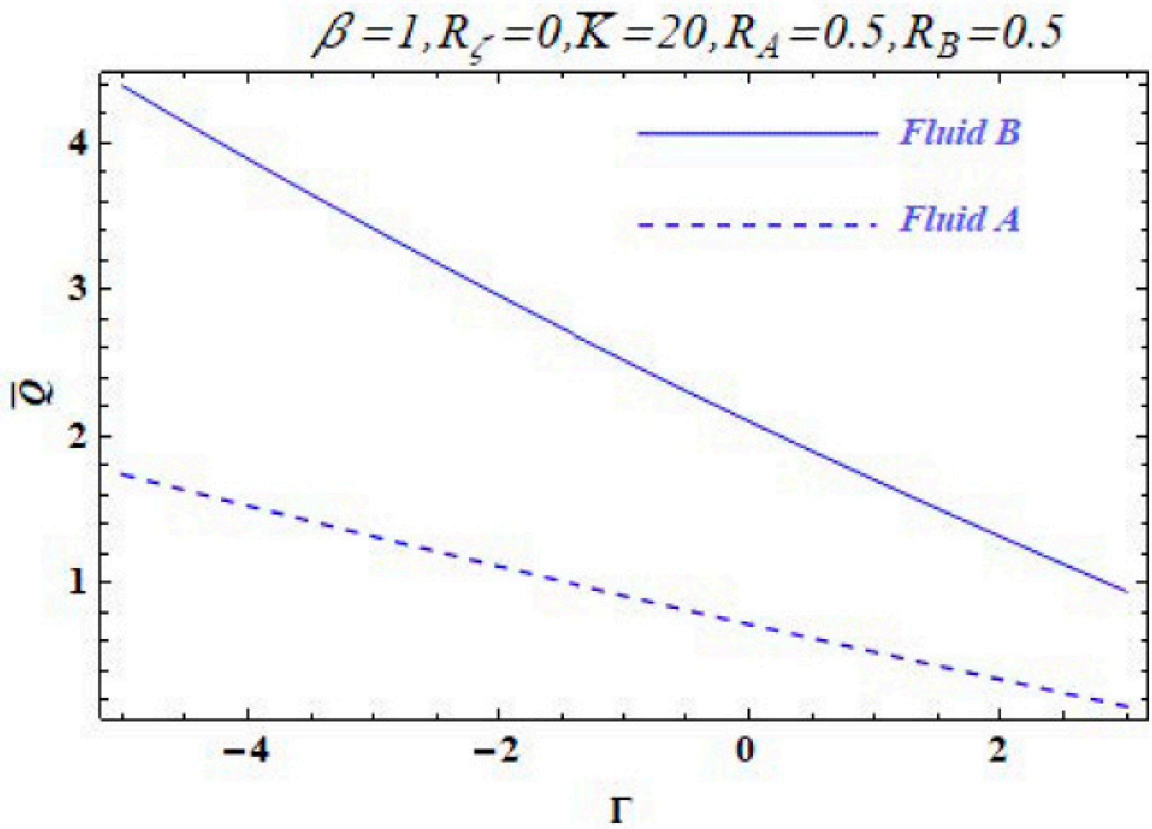

Figure 8. Γ *vs* $\overline{Q}$ for Fluid *A* and Fluid *B*.

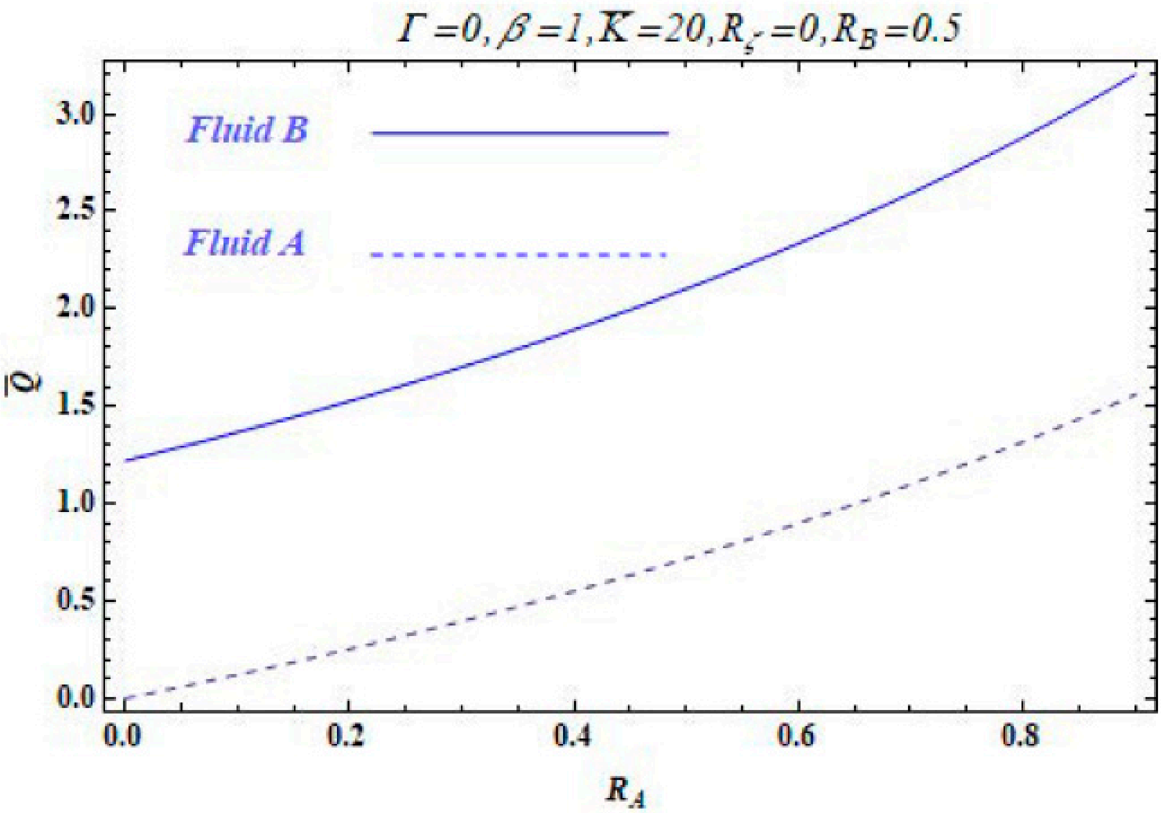

Figure 9. R_A *vs* $\overline{Q}$ for Fluid *A* and Fluid *B*.

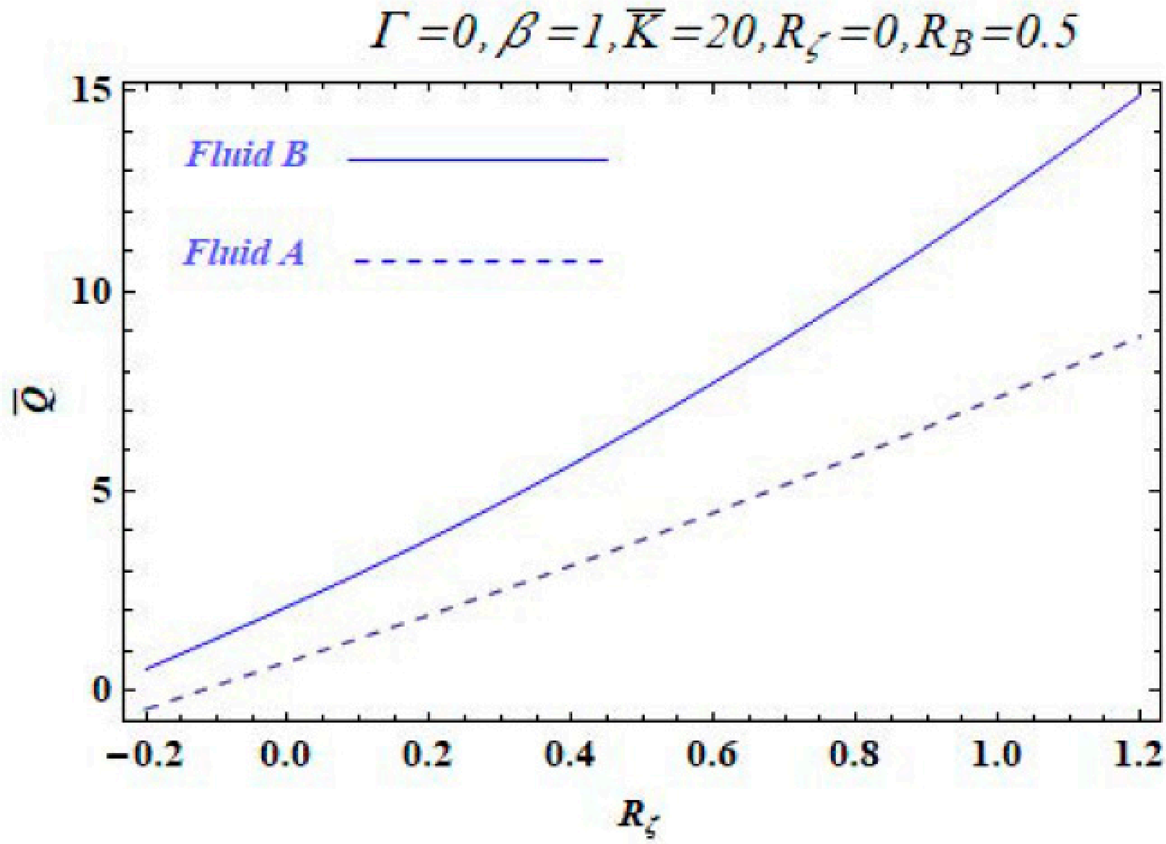

Figure 10. R_ζ *vs* $\overline{Q}$ for Fluid *A* and Fluid *B*.

4. Conclusions

The electro-osmotic flow of two immiscible fluids, which satisfied the Ellis constitutive laws, has been analyzed. Analytical expressions of the velocity and the flow rate for specific values of Ellis' fluid parameter, α , were reported. Within the limit of infinitesimally small shear stresses, the Ellis model characterizes the apparent viscosity of a shear-thinning fluid without a singularity. In particular, when shear loads are extremely low, this model agrees with Newtonian behavior. It was noted that, in contrast to the PTT equation, the Ellis constitutive equation involves two material constants: α and β_1. In this study, for the specific values of α, both velocity and flow rate are increased with an increase in β_1, in the range $\beta_1 < 0.08$. For the case of fixed β_1, the velocity followed a decreasing trend, with an increase in α. This was also true for the flow rate. However, an opposite trend prevailed for $\beta_1 > 0.08$, and the flow rate significantly increased, with an increase in α.

Author Contributions: Conceptualization, H.A.A., H.Y. and L.S.E.-S.; methodology, R.S. and N.A.S.; software, R.S. and N.A.S.; validation, L.S.E.-S. and S.A.E.-T.; formal analysis, L.S.E.-S.; investigation, H.Y., R.S. and N.A.S.; resources, R.S. and N.A.S.; data curation, S.A.E.-T.; writing—original draft preparation, R.S. and N.A.S.; writing—review and editing, H.A.A., H.Y. and S.A.E.-T.; visualization, L.S.E.-S. and S.A.E.-T.; supervision, H.A.A., H.Y. and S.A.E.-T.; project administration, H.A.A., H.Y. All authors have read and agreed to the published version of the manuscript.

Funding: The authors express their gratitude to Princess Nourah bint Abdulrahman University's Re-searchers, Supporting Project number PNURSP2023R17, Princess Nourah bint Abdulrahman University, Riyadh, Saudi Arabia. This work was supported by the Deanship of Scientific Research, the Vice Presidency for Graduate Studies and Scientific Research, King Faisal University, Saudi Arabia (Grant No. 2425). This study is supported via funding from Prince Sattam bin Abdulaziz University project number (PSAU/2023/R/1444).

Institutional Review Board Statement: Not applicable.

Informed Consent Statement: Not applicable.

Data Availability Statement: Data sharing is not applicable to this article as no new data were created or analyzed in this study.

Acknowledgments: The authors express their gratitude to Princess Nourah bint Abdulrahman University Researchers, Supporting Project number (PNURSP2023R17), Princess Nourah bint Abdulrahman University, Riyadh, Saudi Arabia. This work was supported by the Deanship of Scientific Research, the Vice Presidency for Graduate Studies and Scientific Research, King Faisal University, Saudi Arabia (Grant No. 2425). This study is supported via funding from Prince Sattam bin Abdulaziz University project number (PSAU/2023/R/1444).

Conflicts of Interest: The authors declare that they have no conflict of interest.

References

1. Wang, X.; Cheng, C.; Wang, S.; Liu, S. *Electro-Osmotic Pumps and Their Applications in Microfluidic Systems*; Springer: Berlin/Heidelberg, Germany, 2009; Volume 6, pp. 145–162.
2. Brask, A.; Goranovic, G.; Bruus, H. Electro-osmotic pumping of non-conducting liquids by viscous drag from a secondary conducting liquid. *Tech. Proc. Nanotech.* **2003**, *1*, 190–193.
3. Das, S.; Chakraborty, S. Anal. Chim, Electro-osmotic and pressure driven flow of viscoelastic fluids in micro channel. *Acta* **2006**, *559*, 15–24.
4. Chakraborty, S. Electro-osmotically driven capillary transport of typical non-Newtonian bio fluids in rectangular micro channel. *Anal. Chim. Acta* **2007**, *605*, 175–184. [CrossRef] [PubMed]
5. Afonso, A.; Alves, M.; Phino, F. Analytical solution of mixed electroosmotic/pressure driven flows of viscoelastic fluids in microchannels. *J. Non-Newton. Fluid Mech.* **2009**, *159*, 50–63. [CrossRef]
6. Park, H.; Lee, W. Effect of viscoelasticity on the flow pattern and the volumetric flow rate in electro-osmotic flows through a microchannel. *Lab A Chip* **2008**, *8*, 1163–1170. [CrossRef] [PubMed]
7. Afonso, A.; Alves, M.; Phino, F. Elecro-osmotic flow of viscoelastic fluids in microchannel under asymmetric zeta potentials. *J. Eng. Math.* **2011**, *71*, 15–30. [CrossRef]
8. Sousa, J.; Afonso, A.; Alves, M.; Phino, F. Effect of the skimming layer electroosmotic poiseuille flows of viscoelastic fluids. *Microfluid. Nanofluidics* **2011**, *10*, 107–122. [CrossRef]

9. Dhinakaran, S.; Afonso, A.; Alves, M.; Phino, F. Steady viscoelastic fluid flow between parallel plate under electro-osmotic forces. *J. Colloid Interf. Sci.* **2010**, *344*, 513–520. [CrossRef] [PubMed]
10. Afonso, A.; Alves, M.; Phino, F. Electro-osmosis of viscoelastic and prediction of electro-elastic flow instabilities in a cross slot using a finite-volume method. *J. Non-Newton. Fluid Mech.* **2012**, *179*, 55–68. [CrossRef]
11. Afonso, A.; Alves, M.; Phino, F. Analytical solution of two-fluid electro osmotic flows of viscoelastic fluid. *J. Colloid Interface Sci.* **2013**, *395*, 277–286. [CrossRef]
12. Martínez, L.; Bautista, O.; Escandón, J.; Méndez, F. Electroosmotic flow of a Phan-Thien–Tanner fluid in a wavy-wall microchannel. *Colloids Surf. A Physicochem. Eng. Asp.* **2016**, *498*, 7–19. [CrossRef]
13. Deng, S. Analytical Study of the Electroosmotic Flow of Two Immiscible Power-Law Fluids in a Microchannel. *Open J. Fluid Dyn.* **2022**, *12*, 263–276. [CrossRef]
14. Mustafa, T. Eyring–Powell fluid flow through a circular pipe and heat transfer: Full solutions. *Int. J. Numer. Methods Heat Fluid Flow* **2020**, *30*, 4765–4774. [CrossRef]
15. Javed, M.; Ali, N.; Sajid, M. A theoretical analysis of the calendering of Ellis model. *J. Plast. Sheeting* **2017**, *33*, 207–226. [CrossRef]
16. Hayat, T.; Yasmin, H.; Alsaedi, A. Convective heat transfer analysis for peristaltic flow of power-law fluid in a channel. *J. Braz. Soc. Mech. Sci. Eng.* **2015**, *37*, 463–477. [CrossRef]
17. Yasmin, H.; Iqbal, N. Convective mass/heat analysis of an electroosmotic peristaltic flow of ionic liquid in a symmetric porous microchannel with soret and dufour. *Mathe. Prob. Eng.* **2021**, *2021*, 2638647. [CrossRef]
18. Balachandran, P. *Fundamental of Compressible Fluid Dynamics*; Phi Publishers: Delhi, India, 2006.